PERGAMON

Computers & Geosciences 29 (2003) 301–318

COMPUTERS & GEOSCIENCES

www.elsevier.com/locate/cageo

Reactive transport in surface sediments. II. Media: an object-oriented problem-solving environment for early diagenesis

Filip J.R. Meysman[a,*], Jack J. Middelburg[b], Peter M.J. Herman[b], Carlo H.R. Heip[b]

[a] *Marine Biology Department, Ghent University, K.L. Ledeganckstraat 35, Gent 9000 , Belgium*
[b] *The Netherlands Institute of Ecology (NIOO-KNAW), Korringaweg 7, Yerseke 4401 NT, The Netherlands*

Received 1 December 2001; received in revised form 22 May 2002; accepted 22 May 2002

Abstract

The MEDIA (Modelling Early DIAgenesis) software package comprises a flexible and extensible software system that provides problem-solving assistance for simulating 1D reactive transport in surface sediments. MEDIA allows multiple diagenetic models to be built by extending a model template with new model components from a toolbox of available objects (elements, species, parameters, reactions). A detailed review is given of the transport and reaction components available for model construction. Upon assemblage, the model is channelled to the numerical subunit of the MEDIA package. Via a canonical transformation, the user-defined mixed kinetic-equilibrium model is rearranged into a proper set of differential algebraic equations (DAE), for which both steady state and transient solutions can be calculated. Steady-state profiles are obtained either directly using a Newton–Raphson method, or alternatively, as the asymptotic result of a dynamic simulation. Dynamic simulations involve a global implicit procedure based on the stiff-ODE solver package VODE, employing a direct substitution approach to reduce the number of equations in the DAE system. Verification of the MEDIA code was accomplished (1) by comparison with analytic models and (2) by emulating the model formulation and output of the existing diagenetic model code STEADYSED. As an example application, a diagenetic model was constructed to analyse an extensive dataset collected from a marine sediment in the Santa Barbara Basin (California). The different pathways of organic matter mineralization were modelled, and the coupling among the biogeochemical cycles of C, O, N, S, Mn and Fe was investigated. Depth profiles of both porewater and solid-phase constituents could be reproduced with great accuracy.

Keywords: Reactive transport modelling; Early diagenesis; Biogeochemical cycling; Mixed kinetic-equilibrium problem; Direct substitution approach

1. Introduction

In recent years, a number of studies have illustrated the capabilities of sophisticated reactive transport codes for the integrated modelling of biogeochemical cycles in surface sediments (Soetaert et al., 1996b; Wang and Van Cappellen, 1996; Boudreau et al., 1998; Herman et al., 2001). Although powerful applications, current numerical model codes have a number of severe limitations, as

*Corresponding author. Present address: The Netherlands Institute of Ecology (NIOO-KNAW), Korringaweg 7, Yerseke 4401 NT, The Netherlands. Tel.: +31-113-577-489; fax: +31-113-573-616.

E-mail address: f.meysman@nioo.knaw.nl (F.J.R. Meysman).

0098-3004/03/$ - see front matter
doi:10.1016/S0098-3004(03)00007-4

evaluated in a companion paper (Meysman et al., 2002). (1) Model codes are problem-specific, as they incorporate a fixed set of species and reactions, which restricts the type of problems and environments to be investigated. (2) Model codes lack flexibility and extendibility, and the associated need for ground-level reprogramming and recompilation constitutes a major barrier for potential model users. A grand challenge therefore is to encapsulate the present know-how into user-friendly and flexible environments, and to bring this problem-solving power within reach of geochemists that are not familiar with computational issues.

Meeting this challenge constitutes the central philosophy behind the (MEDIA) (Modelling Early DIAgenesis) software package, which is built on two fundamental strongholds: (1) Problem-Solving Environments (PSE), a modern concept from the field of Computational Science and Engineering (CSE) (Ford and Chatelin, 1987; Gallopoulos et al., 1994) and (2) Object-Oriented Technology (OOT), the recent paradigm from the field of Industrial Software Engineering (Booch, 1994; Page-Jones, 2000). Both techniques enhance the software quality of reactive transport codes, and consequently, they lower the threshold for using diagenetic model codes as a routine instrument for geochemical data analysis. The implementation of PSE and OOT in the design and structure of the MEDIA software (i.e. the issues of concern to *software developers*) has been described in detail in the companion paper (Meysman et al., 2002). In this second paper, we will primarily focus on the issues that are of particular interest to *software users*, i.e. the assumptions underlying model construction, numerical methods, verification, and application of MEDIA.

2. Diagenetic model formulation

To conceive a description of the sediment on a macroscopic level, suitable conservation equations must be derived from multi-component, multi-phase continuum physics (Truesdell and Toupin, 1960; Bowen, 1976; Bear and Bachmat, 1991). The application of continuum modelling theory to early diagenesis is discussed in detail in Meysman (2001).[1] Following assumptions have been made: (1) benthic organisms are not explicitly incorporated in the model description as a separate phase, (2) the modelled sediment stratum is shallow (top 10–50 cm) and therefore, it can be considered an isothermal environment, obviating the construction of an energy balance for the porewater and the solid phase, (3) early diagenetic reactions do not appreciably alter the total density of both the fluid and the solid phase, (4) the sediment resides in a steady-state compaction regime, so momentum balances become redundant (5) horizontal gradients in the sediment are less pronounced than vertical gradients, so that the most important diagenetic changes are vertically directed, (6) the sediment is considered laterally homogeneous and (7) the sediment surface does not show any topography. Assumptions (2)–(4) allow us to restrict the description to mass conservation only, while assumptions (5)–(7) justify the conventional 1D-approach of early diagenesis (Berner, 1980). The mass conservation equation for a constituent of the pore water (the fluid phase **f**) or the sediment matrix (the solid phase **s**) is termed the general diagenetic equation (Berner, 1980; Boudreau, 1997; Meysman, 2001):

$$\frac{\partial}{\partial t}[\phi^{\alpha} C_i^{\alpha}] + \frac{\partial}{\partial x}[\phi^{\alpha} v^{\alpha} C_i^{\alpha}] + \frac{\partial}{\partial x}[J_i^{\alpha,dif}] = \Gamma_i^{reac,\alpha} + \Gamma_i^{bio,\alpha}, \quad (1)$$

where ϕ^{α} denotes the volume fraction of phase $\alpha(=\mathbf{f}, \mathbf{s})$, C_i^{α} denotes the concentration of the ith constituent in the α-phase (in molar units), v^{α} denotes the mass-averaged phase velocity, also termed the advective velocity, $J_i^{\alpha,dif}$ represents the total diffusive mass flux with respect to v^{α}, $\Gamma_i^{reac,\alpha}$ represents a source/sink term due to chemical reactions (both homogeneous and heterogeneous) and $\Gamma_i^{bio,\alpha}$ represents a source/sink term due to biologically induced transport. The x-coordinate axis is tied to the sediment–water interface, pointing downwards into the sediment.

By multiplication of Eq. (1) with the appropriate molecular mass M_i^{α} and summation over all species within a particular phase, one obtains a mass balance for the total fluid and the solid phase (Boudreau, 1997). If we assume there is no bulk interphase mass transfer due to either heterogeneous reactions $\left(\sum_i M_i^{\alpha}\Gamma_i^{reac,\alpha} = 0\right)$ or biological activity $\left(\sum_i M_i^{\alpha}\Gamma_i^{bio,\alpha} = 0\right)$, and since the mass density ρ^{α} of both phases is assumed constant, this equation becomes (Berner, 1980; Boudreau, 1997; Meysman, 2001):

$$\frac{\partial[\phi^{\alpha}]}{\partial t} + \frac{\partial}{\partial x}[\phi^{\alpha} v^{\alpha}] = 0. \quad (2)$$

By a suitable combination of Eqs. (2) and (1), the general diagenetic Equation (1) can be brought back to

$$\phi^{\alpha}\frac{\partial C_i^{\alpha}}{\partial t} + L_i^{\alpha}(C_i^{\alpha}) = \Gamma_i^{reac,\alpha}, \quad (3)$$

where the transport operator L_i^{α} comprises a summation of terms, including advective, diffusive and biologically mediated transport (e.g. irrigation, deposit feeding), respectively

$$L_i^{\alpha}(C_i^{\alpha}) = \phi^{\alpha} v^{\alpha}\frac{\partial}{\partial x}[C_i^{\alpha}] + \frac{\partial}{\partial x}[J_i^{\alpha,dif}] - \Gamma_i^{bio,\alpha}. \quad (4)$$

[1] Modelling the Influence of Ecological Interactions on Reactive Transport Processes in Sediments. Online version Ph.D. Dissertation. Meysman, F.J.R., Ghent University, 2001. http://www.nioo.knaw.nl/homepages/meysman/phd_thesis.htm

The reaction set consists of m_{ir} irreversible reactions and m_{rr} reversible reactions

$$0 \rightleftharpoons \sum_{i=1}^{n} v_{i,k}^{ir} A_i, \tag{5}$$

$$0 \rightleftharpoons \sum_{i=1}^{n} v_{i,l}^{rr} A_i, \tag{6}$$

where A_i symbolizes the ith chemical species, while $v_{i,k}^{ir}$ and $v_{i,l}^{rr}$ represent the stoichiometric coefficients of A_i in the kth irreversible and the lth reversible reaction, respectively. Stoichiometric coefficients are taken to be positive for a product species and negative for a reactant species. Each reaction, irreversible as well as reversible, can be either homogeneous (taking place wholly within a single phase) or heterogeneous (generating mass transfer between the porewater and the sediment matrix). Introducing the reversible and irreversible reaction rates R_k^{ir} and R_l^{rr} (stated per unit of bulk volume), the reactive source term $\Gamma_i^{reac,\alpha}$ can be calculated as

$$\Gamma_i^{reac,\alpha} = \sum_{k=1}^{m_{ir}} v_{i,k}^{ir} R_k^{ir} + \sum_{l=1}^{m_{rr}} v_{i,l}^{rr} R_l^{rr}. \tag{7}$$

To permit the integration of the diagenetic Equation (3), explicit expressions are needed for both types of reaction rates. Irreversible reaction rates R_k^{ir} are calculated using an appropriate kinetic rate law. The actual form of the kinetic rate law for the different classes of irreversible reactions available within MEDIA is discussed below. In the case of reversible reactions, the rate terms R_k^{rr} are treated as additional unknowns in the diagenetic equations. Employing a partial local equilibrium approach (PLEA), the addition of these extra variables is compensated by an equal number of thermodynamic algebraic equations, specifying the local equilibrium conditions for each of the reversible reactions (Rubin, 1983; Bahr and Rubin, 1987; Lichtner, 1996). The effective PLEA procedure, which rearranges the diagenetic system to remove the unknown reversible reaction rates, is discussed later.

3. The structure of a MEDIA model

Introducing *generic model construction,* MEDIA has been designed to avoid the time-consuming and strenuous tasks of code-writing and debugging as much as possible. Rather than focusing on a single model, different diagenetic models can be constructed within MEDIA without specialized knowledge of the programming language underlying the computer code (i.e. without recompilation). Basically, the application user assembles her/his own diagenetic model from a toolbox of available model components. New components (e.g. new elements, species, parameters, reactions) can be created and added via an object-oriented database. Secondly, it is wittingly anticipated that the present form of the MEDIA software cannot meet all future user demands. In essence, it is impossible to foresee all the specific requirements set by potential application users. Hence, when modification of the code cannot be avoided, the modular structure of the MEDIA code—enforced by its object-oriented design—allows the model user an easy and flexible incorporation of new processes and functions.

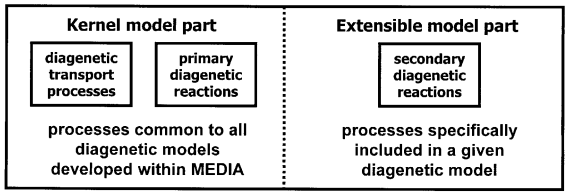

Fig. 1. Structure of MEDIA environment. Each model consists of two parts: a predefined kernel part, which is common to all MEDIA models, and an extensible part, which is specific for model under construction.

To facilitate and accelerate the process of diagenetic model construction, MEDIA provides a basic model template. Each model consists of two separate parts: a predefined *kernel part*, which is common to all MEDIA models, and an *extensible part,* which is specific for the model under construction (Fig. 1). Rather than building models from scratch, the kernel is used as a scaffold for the construction of user-tailored models. Moreover, we recognize that aquatic sediments can be adequately described by the same set of transport processes, while in contrast, the reactive part is highly environment-specific and thus model-specific. Therefore, the kernel includes all diagenetic transport processes, and a small set of reactions that are typical for most early diagenetic problems (so-called primary diagenetic reactions, Tables 2–4; see later). Nevertheless, the application user determines the greater part of species and reactions (so-called secondary diagenetic reactions), i.e. those specific for the problem at hand. So, the crucial task for the MEDIA user is to select the proper building blocks for the extensible model part. An arbitrary number of non-reactive tracer species and reactions can be added (Fig. 2). This way, a wide range of different models can be built within MEDIA without modification of underlying source code (Meysman et al., 2002).

4. Transport processes

To obtain an explicit expression for the transport operator, Eq. (4), constitutive expressions are required for the volume fraction ϕ^{α}, the phase velocity v^{α}, the

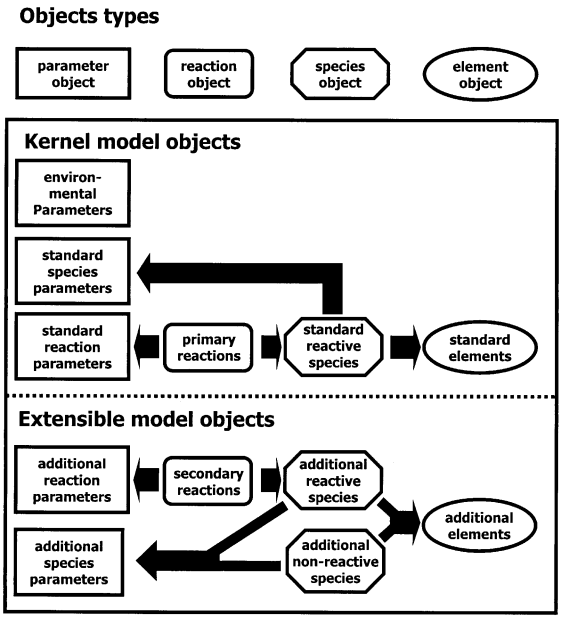

Fig. 2. Overview of linkage among four different types of objects within MEDIA. Environmental parameters are included by default in model kernel. Primary reactions included in model kernel give rise to an associated set of standard reactive species and reaction parameters. In their turn, standard reactive species are associated with a set of standard species parameters and a set of standard elements. Addition of user-selected reactions to extensible part of MEDIA may require incorporation of additional reactive species, if these are not already present in object database. Similarly, these species—together with additional non-reactive species—may require incorporation of a set of additional elements and additional species parameters.

diffusive flux $J_i^{\alpha,dif}$ and the biological source/sink term $\Gamma_i^{bio,\alpha}$.

The differential equation for the volume fraction, Eq. (2), can be made redundant through the assumption of steady-state compaction, which implies that the porosity ϕ^f (or equally the solid volume fraction $\phi^s = 1 - \phi^f$) is invariant with time (Boudreau, 1997):

$$\frac{\partial \phi^\alpha}{\partial t} = 0. \tag{8}$$

However, when performing dynamic simulations, the assumption of steady-state compaction can be rightly put into question. Firstly, sediment porosity can be altered due to water–rock interactions (Berner, 1980; Ortoleva et al., 1987), yet, the associated time-scale of this process is generally longer than that of early diagenesis (from $\sim$50 yr in coastal sediments to $\sim$5000 yr in deep-sea sediments). More important for surficial sediments are the potential porosity changes due to biological reworking of the sediment by macrofauna (Rhoads, 1974; Aller, 1982). Unfortunately,

Table 1
Parameterizations for a general parameter θ as a function of depth

1. Constant
$\theta(x) = \theta_0$ when $x \leqslant x^\theta$
$\theta(x) = \theta_\infty$ when $x > x^\theta$

2. Linear
$\theta(x) = \theta_\infty + (\theta_0 - \theta_\infty)\left[1 - \frac{x}{x^\theta}\right]$ when $x \leqslant x^\phi$
$\theta(x) = \theta_\infty$ when $x > x^\phi$

3. Exponential
$\theta(x) = \theta_\infty + (\theta_0 - \theta_\infty)\exp(-x/x^\theta)$

4. Inverse exponential
$\theta(x) = \frac{\theta_0 \theta_\infty}{\theta_0 + (\theta_\infty - \theta_0)\exp(-x/x^\theta)}$

Each mathematical expression possesses the general form $\theta = \theta(x, \theta_o, \theta_\infty, x^\theta)$ where θ denotes a general parameter. Three parameter values need to be assigned on input: θ_0 represents value at sediment-water interface, θ_∞ denotes value at infinite depth and x^θ constitutes a characteristic depth (used as an attenuation constant for depth profile).

considerable debate subsists on how animals actually influence porosity profiles, and hence, a consistent description of biological porosity alterations appears to be lacking (Mulsow et al., 1998). Pragmatically, and following the conventional approach (Berner, 1980; Soetaert et al., 1996a; Boudreau, 1996a, 1997 Van Cappellen and Wang, 1996), we adopt steady-state compaction and do not incorporate volume fractions ϕ^α as true diagenetic variables. Consequently, an empirical expression is needed to describe this porosity depth profile (e.g. exponential in Rabouille and Gaillard (1991) and Soetaert et al. (1996a); inverse exponential in Boudreau and Bennett (1999)). To allow a wide range of profiles, MEDIA provides a number of different parameterizations (constant, linear, exponential and inverse exponential) as depicted in Table 1. Similar functionalities are used to model the depth dependency of other model parameters.

Due to the assumption of steady-state compaction, Eq. (8), the phase mass balance, Eq. (2), simplifies to

$$\frac{\partial}{\partial x}[\phi^\alpha v^\alpha] = \frac{\partial}{\partial x}\left[\frac{F^\alpha}{\rho^\alpha}\right] = 0, \tag{9}$$

which implies that the total mass flux $F^\alpha = \phi^\alpha \rho^\alpha v^\alpha$ in both the pore water and solid phase remains constant with depth. Given the constant phase density ρ^α and the prescribed depth profile $\phi^\alpha(x)$, then fixing the flux F^α through the sediment–water interface, will completely determine the depth profile of the phase velocity $v^\alpha(x)$. In the situation of solids, the flux F^s is provided at the upper boundary, i.e. as part of the input information

(see for example Table 6). To calculate the pore water flux F^f, an additional assumption has to be made about the actual flow field in the sediment. When there is no forced porewater flow, one can assume that both the solids and pore water are 'buried' with the same velocity $v^f_\infty = v^s_\infty$ at infinity depth. Then the total pore water flux can be calculated as $F^f = \phi^f_\infty \rho^f v^f_\infty$. When externally impressed flow is important (due to seepage of groundwater or hydrothermal vents), the advective velocity u of the pore water at the base of the modelled sediment layer ($x = L$) needs to be specified $v^f_L = u$ as part of the input information. In the latter situation, the total pore water flux can be calculated as $F^f = \phi^f_L \rho^f u$.

Diffusive processes cause the velocity of individual components to deviate from the (mass-averaged) phase velocity, resulting in the diffusive flux $J^{\alpha,dif}_i$. In most early diagenetic environments, hydrodynamic dispersion can be neglected due to low pore water velocities. Hence, the diffusive flux $J^{\alpha,dif}_i$ is written as a sum of three parts: molecular diffusion (*md*), dispersion due to surface waves and currents (*wd*), and biological mixing (*b*)

$$J^{\alpha,dif}_i = J^{\alpha,md}_i + J^{\alpha,wd}_i + J^{\alpha,b}_i.$$

In most pore waters, molecular diffusion sufficiently resembles the process in dilute solutions (Boudreau, 1997). As a consequence, the simple formalism of Fick's First Law is used for the flux due to molecular diffusion:

$$J^{f,md}_i = -\phi^f D^{md}_i \frac{\partial C^f_i}{\partial x}. \tag{10}$$

The effective molecular diffusion coefficient D^{md}_i is species-dependent and must be calculated as a function of the temperature T (K), the pressure p (bar) and salinity S (PSU). Boudreau (1997) provides a detailed account of such a procedure for the ions and molecules frequently encountered in early diagenetic models. This procedure can be summarized as

$$D^{md}_i(x) = \frac{1}{\theta^2(x)} \frac{\mu(S_0,P_0)}{\mu(S,P)} \times [D^0_i(T_0,S_0,P_0) + a_i(T - T_0)], \tag{11}$$

where D^0_i is the infinite dilution diffusion coefficient (specified at a reference temperature T_0, a reference pressure P_0 and reference salinity S_0) and a_i is the attenuation constant in a linear temperature correction. Furthermore, a correction for salinity S and pressure P is implemented using the Stokes–Einstein relationship for the pore water viscosity μ (Boudreau, 1997). Finally, the diffusion coefficient is corrected for the geometry of the porous medium introducing the tortuosity factor θ. Boudreau (1996b) advocates the modified Wiessberg equation as an adequate description over the range of porosity values commonly encountered in surface sediments:

$$\theta^2(x) = 1 - \ln(\phi(x)^2). \tag{12}$$

Subtidal waves and currents induce pressure variations at the sediment–water interface, which result in pore water fluctuations in the sediment bed (Madsen, 1978, Jeng et al., 2000). In a flat bed—as assumed by our 1D approach—the flow trajectories are closed and consequently, there is no net advection (Shum and Sundby, 1996). The effect of wave- or current-induced porewater motion on solute transport then can be treated as a diffusive phenomenon (van der Loeff, 1981; Harrison et al., 1983)

$$J^{f,wd}_i = -\phi^f D^{wd} \frac{\partial C^f_i}{\partial x}, \tag{13}$$

where the dispersion coefficient D^{wd} is specified using the parameter profiles of Table 1.

Bioturbation is the mixing of the sediments due to the activity of organisms, which includes the internal mixing of both pore water and solid phase. The common approach is to model biological mixing through a Fickian formulation (Goldberg and Koide, 1962; Guinasso and Schink, 1975; Boudreau, 1986):

$$J^{b,f}_i = -\phi^f (D^{en} + D^b) \frac{\partial C^f_i}{\partial x}, \tag{14}$$

$$J^{b,s}_i = -\phi^s D^b \frac{\partial C^s_i}{\partial x} \tag{15}$$

and this introduces two distinct bioturbation coefficients. The coefficient D^b represents the mixing of both sediment and porewater by macrofauna (e.g. Aller and Yingst, 1985). The coefficient D^{en} incorporates the enhanced mixing of the pore water by smaller organisms, like meiofauna (Aller and Aller, 1992) and microzoobenthos (Glud and Fenchel, 1999). As both coefficients reflect the presence of benthic organisms, they are allowed to vary with depth (using the parameter profiles of Table 1).

Irrigation by tube-dwelling organisms may add significantly to surficial transport in sediments inhabited by macrofauna (e.g. Archer and Devol, 1992; Aller and Aller, 1998). A source/sink formulation is adopted, which provides a 1D analogue for the enhancement of diffusion due to burrows in a 3D sediment setting (Boudreau, 1984; Emerson et al., 1984).

$$\Gamma^{bio,f}_i = \alpha(C^{wc}_i - C^f_i), \tag{16}$$

where C^{wc}_i represents the concentration in the overlying water column and $\alpha(x)$ the irrigation coefficient (also specified by the parameterizations of Table 1). Biological transport for solid species—so-called non-local transport (Boudreau, 1986)—is not incorporated at present. However, due to the modular structure of the code, the MEDIA software is easily altered to accommodate new transport processes.

5. Boundary and initial conditions

To complete the model formulation, boundary conditions are stated both at the *sediment–water interface* (SWI at $x = 0$), and at the base of the model, which is termed the *lower sediment interface* (LSI at $x = L$). A wide range of boundary conditions is available to the user, including Dirichlet (concentration), Neumann (gradient) and Robin's (mixed) conditions, as described in detail in Meysman (2001) and the MEDIA's user manual.[2] Boundary parameters (as well as other input parameters) can be constant or time-dependent. The temporal variation of parameters is implemented via small forcing modules (small, additional pieces of code by which the user defines an arbitrary complex functionality of time).

Besides boundary conditions, the model must be supplied with appropriate initial conditions. When a steady state is calculated as the asymptotic limit of a dynamical simulation, an adequate set of initial conditions (i.e. sufficiently close to the final steady state) can significantly reduce the simulation time. Initial concentration profiles can be implemented in two different ways: (1) MEDIA allows the input of a set of concentration profiles that are obtained as the output from a previous simulation and (2) if such a set of profiles is not available, rough initial values are estimated from the upper boundary conditions. In the case of a fixed concentration $C^{\alpha}_{i,o}$ at the upper boundary, then the initial profile uniformly adopts the boundary concentration $C^{\alpha}_{i}(x,0) = C^{\alpha}_{i,o}$. In situations where a fixed flux $F^{\alpha}_{i,o}$ has been adopted, a uniform concentration profile is calculated as $C^{\alpha}_{i}(x,0) = F^{\alpha}_{i,o}/(\phi^{\alpha}_{o} v^{\alpha}_{o})$.

6. The reaction kernel

The MEDIA kernel includes a basic set of reactions, termed *primary diagenetic reactions,* presently consisting of three classes. (1) Organic matter *mineralization reactions* constitute the driving force of early diagenesis. (2) *Dissociation reactions* account for all major acid–base equilibria in natural waters. (3) *Sorption reactions* describe the sorption of freshly produced mineralization products onto the sediment matrix.

6.1. Mineralization reactions

Organic matter (OM) is divided into reactive fractions OM_j, whose stoichiometric composition (C/N/P ratio) is given by the coefficients x_j,y_j and z_j, respectively (Westrich and Berner, 1984):

$$\mathrm{OM}_j = \{\mathrm{CH_2O}\}_{x_j}\{\mathrm{NH_3}\}_{y_j}\{\mathrm{H_3PO_4}\}_{z_j}. \tag{17}$$

The mineralization pathways of each organic matter fraction include oxic mineralization, denitrification, oxidation by manganese and iron (hydr)oxides, sulphate reduction and methanogenesis (Froelich et al., 1979; Table 2, reactions [M1–M6], Fig. 3). The mineralization rate $R^{mi}_{i,j}$ represents the oxidation rate of the OM_j fraction by the ith pathway:

$$R^{mi}_{i,j} = x_j k^{mi}_{j}[\mathrm{OM}_j]\frac{[\mathrm{O}x_i]}{[\mathrm{O}x_i] + K^{i}_{S}}\prod_{m=1}^{i-1}\frac{K^{m}_{I}}{[\mathrm{O}x_m] + K^{m}_{I}}. \tag{18}$$

These so-called modified Monod kinetics comprise the conventional description of organic matter mineralization in early diagenetic models (Van Cappellen et al., 1993; Van Cappellen and Wang, 1996; Soetaert et al., 1996a; Boudreau, 1996a). The importance of a particular pathway is dependent on a combination of three terms: (1) substrate limitation is modelled via the first-order decay constant k^{mi}_{j} of the jth fraction OM_j, (2) the limitation of the oxidant $\mathrm{O}x_i$ is represented by a Monod-type hyperbolic expression involving the half-saturation constant K^{i}_{S} and (3) the repression of the ith pathway by energetically more favourable oxidants $\mathrm{O}x_m$ is modelled by an inhibition-type function involving the inhibition constant K^{m}_{I}.

Traditionally, no intermediates of the OM mineralization process (molecular hydrogen, acetate, etc.) are explicitly modelled. However, molecular hydrogen was recently demonstrated as a reaction side-product in the formation of pyrite (Drobner et al., 1990; Rickard and Luther, 1997), i.e. the end product of a non-mineralization reaction. To prevent molecular hydrogen from accumulating in the model, its consumption as a highly reactive intermediate in the process of organic matter degradation (Fig. 3) must be incorporated. The same set of electron acceptors—i.e. oxygen, nitrate, manganese oxide, iron oxide, and sulphate—were coupled to the oxidation of hydrogen (Table 2, reactions [M7]–[M11]). The rate $R^{H_2}_{i}$ of a particular pathway of hydrogen oxidation is modelled by a similar expression as Eq. (18):

$$R^{H_2}_{i} = k_{H_2}[\mathrm{H_2}]\frac{[\mathrm{O}x_i]}{[\mathrm{O}x_i] + K^{i}_{S}}\prod_{m=1}^{i-1}\frac{K^{m}_{I}}{[\mathrm{O}x_m] + K^{m}_{I}}, \tag{19}$$

where k_{H_2} is now the decay constant of molecular hydrogen. The same half-saturation and inhibition constants are used as in Eq. (18).

6.2. Dissociation reactions

The speciation and pH of porewaters are affected by various acid–base equilibria. The MEDIA model includes all equilibria that are considered important in the acid–base behaviour of seawater i.e. the carbonate,

[2] MEDIA online manual. http://www.nioo.knaw.nl/homepages/meysman/media.htm

Table 2
Mineralization reactions included in MEDIA kernel

Mineralization reactions of organic matter

$$[CH_2O]_x[NH_3]_y[H_3PO_4]_z + xO_2 + yH^+ \rightarrow xCO_2 + yNH_4^+ + zHPO_4^{2-} + 2zH^+ + xH_2O \quad [M1]$$

$$[CH_2O]_x[NH_3]_y[H_3PO_4]_z + \frac{4x}{5}NO_3^- + \frac{4x+5y}{5}H^+ \rightarrow xCO_2 + yNH_4^+ + zHPO_4^{2-} + 2zH^+ + \frac{4x}{5}N_2 + \frac{7x}{5}H_2O \quad [M2]$$

$$[CH_2O]_x[NH_3]_y[H_3PO_4]_z + 2MnO_2 + [4x+y]H^+ \rightarrow xCO_2 + yNH_4^+ + zHPO_4^{2-} + 2zH^+ + 2Mn^{2+} + 3xH_2O \quad [M3]$$

$$[CH_2O]_x[NH_3]_y[H_3PO_4]_z + 4xFeOOH + [8x+y]H^+ \rightarrow xCO_2 + yNH_4^+ + zHPO_4^{2-} + 2zH^+ + 4xFe^+ + 7xH_2O \quad [M4]$$

$$[CH_2O]_x[NH_3]_y[H_3PO_4]_z + \frac{x}{2}SO_4^{2-} + \frac{x+2y}{2}H^+ \rightarrow xCO_2 + yNH_4^+ + zHPO_4^{2-} + 2zH^+ + \frac{x}{2}HS^- + xH_2O \quad [M5]$$

$$[CH_2O]_x[NH_3]_y[H_3PO_4]_z + yH^+ \rightarrow \frac{x}{2}CO_2 + yNH_4^+ + zHPO_4^{2-} + 2zH^+ + \frac{x}{2}CH_4 \quad [M6]$$

Mineralization reactions involving hydrogen

$$H_2 + \frac{1}{2}O_2 \rightarrow H_2O \quad [M7]$$

$$H_2 + \frac{1}{4}NO_3^- + \frac{1}{2}H^+ \rightarrow \frac{1}{4}NH_4^+ + \frac{3}{4}H_2O \quad [M8]$$

$$H_2 + MnO_2 + 2H^+ \rightarrow Mn^{2+} + 2H_2O \quad [M9]$$

$$H_2 + 2FeOOH + 4H^+ \rightarrow 2Fe^{2+} + 4H_2O \quad [M10]$$

$$H_2 + \frac{1}{4}SO_4^{2-} + \frac{1}{2}H^+ \rightarrow \frac{1}{4}H_2S + 2H_2O \quad [M11]$$

$$H_2 + \frac{1}{4}CO_2 \rightarrow \frac{1}{4}CH_4 + \frac{3}{4}H_2O \quad [M12]$$

sulphide, phosphate, ammonium, sulphide, borate and silicate acid–base dissociation reactions (Table 3, reactions [D1]–[D8]). These reactions are modelled as in local equilibrium and the apparent dissociation constants are calculated as a function of temperature, pressure and salinity using the relations of Millero (1995). There is some evidence that porewater equilibria alone are not sufficient for a full understanding of porewater pH (e.g. Wang and Van Cappellen, 1996), and thus additional equilibria involving the solid matrix must be taken into account. To this effect, the acid–base behaviour of the detrital clay fraction was modelled as a two-step dissociation reaction for hydroxyl sites at the fluid–solid interface (Table 3, reactions [D9]–[D10]). The apparent dissociation constants for the latter two reactions must be provided as input data.

6.3. Sorption reactions

Sorption processes are considered fast relative to the characteristic time scales of the transport processes. Hence, an equilibrium formulation is used to describe the partitioning between the pore water and the surface sites of the sediment matrix. A linear adsorption formulation is included for ammonium (Rosenfeld, 1979; Mackin and Aller, 1984; Soetaert et al., 1996a; Van Cappellen and Wang, 1996; Boudreau, 1996a) and phosphate species (Krom and Berner, 1980; Boudreau, 1996a) (Table 4, reactions [S1]–[S4]). The adsorption of the metal ions Fe^{2+}, Mn^{2+} and Mg^{2+} is modelled via a non-linear formulation, since it is assumed that the sorption capacity for these cations correlates with the presence of iron and manganese (hydr)oxides that have reactive surface areas (Canfield et al., 1993; Van Cappellen and Wang, 1996) (Table 4, reactions [S5]–[S7]). We have implemented a slightly modified version of the competitive adsorption model presented by Van Cappellen and Wang (1996). Rather than modelling an unspecified cation concentration, we have introduced Mg^{2+} as the species in competitive equilibrium with Mn^{2+} and Fe^{2+}. Mg^{2+} is the dominant divalent cation in marine porewaters, and thus we employed it to emulate the influence of cations on the sorption equilibria of Mn^{2+} and Fe^{2+}.

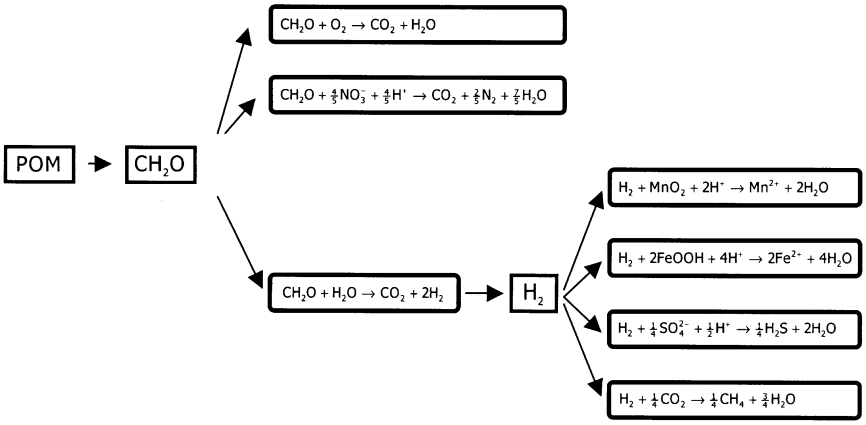

Fig. 3. Overall process of organic matter degradation modelled as a set of idealized biochemical transformations. A cascaded multi-step mechanism is proposed, where first step comprises hydrolization of particulate organic matter (POM) into monomers like simple sugars and amino acids (represented asCH_2O). Second step depends on terminal electron acceptors (TEAs) involved. In example of oxygen and nitrate, most probable pathway is direct oxidation of monomers to carbon dioxide. For other TEAs, intermediate fermentation of monomers is considered, producing small organic molecules such as H_2 acetate and formate (Lovley and Chapelle, 1995) (only H_2 is shown). Subsequently, these intermediate fermentation products are consumed in a series of terminal electron acceptor processes, involving manganese (hydr)oxides, iron (hydr)oxides, sulphate and finally carbon dioxide itself.

Table 3
Dissociation reactions included in MEDIA kernel

Dissociation reactions in the porewater	
$H_2O \rightleftharpoons OH^- + H^+$	[D1]
$CO_2 + H_2O \rightleftharpoons HCO_3^- + H^+$	[D2]
$HCO_3^- \rightleftharpoons CO_3^{2-} + H^+$	[D3]
$H_2PO_4^- \rightleftharpoons HPO_4^{2-} + H^+$	[D4]
$HPO_4^{2-} \rightleftharpoons PO_4^{3-} + H^+$	[D5]
$NH_4^+ \rightleftharpoons NH_3 + H^+$	[D6]
$H_2S \rightleftharpoons HS^- + H^+$	[D7]
$B(OH)_3 + H_2O \rightleftharpoons B(OH)_4^- + H^+$	[D8]
$Si(OH)_4 \rightleftharpoons SiO(OH)_3^- + H^+$	[D9]
Dissociation reactions involving the solid sediment matrix	
$\equiv OH_2^+ \rightleftharpoons \equiv OH + H^+$	[D10]
$\equiv OH \rightleftharpoons \equiv O^- + H^+$	[D11]

Table 4
Sorption reactions included in MEDIA kernel

Sorption reactions involving nutrients	
$NH_4^+ \rightleftharpoons \equiv NH_4^+$	[S1]
$HPO_4^{2-} \rightleftharpoons \equiv HPO_4^{2-}$	[S2]
$2PO_4^- \rightleftharpoons \equiv H_2PO_4^-$	[S3]
$PO_4^{3-} \rightleftharpoons \equiv PO_4^{3-}$	[S4]
Sorption reactions involving metal ions	
$\equiv H + Mn^{2+} \rightleftharpoons \equiv Mn^+ + H^+$	[S5]
$\equiv H + Fe^{2+} \rightleftharpoons \equiv Fe^+ + H^+$	[S6]
$\equiv H + Mg^{2+} \rightleftharpoons \equiv Mg^+ + H^+$	[S7]

7. The extensible reaction set

By extending the kernel reaction set, the modeller can tailor a diagenetic model to the problem being addressed. Those reactions, which can be freely chosen by the modeller, are termed *secondary diagenetic reactions* and are included in the extensible part of the reaction set. Unlike the kernel reaction set, the extensible reaction set constitutes an open reaction set. Hence, the user can add new reactions to each class in the object database, which subsequently become available for model construction. When a new reaction is added to a reaction class, this reaction will receive the kinetic rate law of the corresponding reaction class. In the MEDIA software (available online), each reaction class in the object database already includes a number of example reactions. Five different classes of secondary reactions are presently available (Table 5), which reflect the kinetic formulations frequently encountered in early diagenetic models (Boudreau, 1996a; Van Cappellen and Wang, 1996). More sophisticated kinetic formulations (surface area effects, pH dependencies etc.) can be added by the model user as a new class. This requires an extension of the software with a small module that specifies the mathematical expression of the desired kinetic formula.

7.1. Fluid redox reactions

This class (denoted *fr*) includes the homogeneous redox reactions occurring wholly within the porewater

Table 5
Overview of different classes available in MEDIA reaction set

Reaction class	Description	Class type	Number
Mineralization reactions	Kinetic	Kernel class	12
Acid-base dissociation reactions	Equilibrium	Kernel class	11
Sorption reactions	Equilibrium	Kernel class	7
Fluid redox reactions	Kinetic	Extensible class	User-determined
Surface redox reactions	Kinetic	Extensible class	User-determined
Pseudo solid phase reactions	Kinetic	Extensible class	User-determined
Precipitation reactions	Kinetic	Extensible class	User-determined
Dissolution reactions	Kinetic	Extensible class	User-determined

MEDIA model kernel includes 30 reactions, of which 12 receive a kinetic description (mineralization reactions) and 18 receive an equilibrium description (dissociation and sorption reactions). Extensible classes all receive a kinetic description.

fluid. The reaction rate R^{fr} (defined per volume of porewater) is expressed as a rate law based on the product of concentration terms (Lasaga, 1997):

$$R^{fr} = k^{fr} \prod_i (C_i^f)^{v_i}, \tag{20}$$

where $k^{fr}$is the rate constant, C_i^f represents a solute concentration and v_i is a real exponent.

7.2. Surface redox reactions

This class (denoted *sr*) incorporates heterogeneous redox reactions that occur at the surface of the sediment particles. The reaction rate R^{sr} (defined per volume of porewater) is expressed via a similar rate law as Eq. (20), but now the reactive surface area of the mineral must be taken into account (Lasaga, 1997):

$$R^{sr} = k^{sr} A_j^s \prod_i [C_i^f]^{v_i}, \tag{21}$$

where k^{sr} is the rate constant, C_i^f represents a solute concentration, A_j^s represents the reactive surface area of the jth solid species per volume of porewater (it is assumed only one mineral is taking part in the reaction), while v_i constitutes a real exponent. The reactive surface area is expressed in terms of the concentration of the solid species via

$$A_j^s = \frac{\phi^s}{\phi^f} \rho^s \frac{S_j^s}{M_j^s} C_j^s, \tag{22}$$

where $\phi^s$is the volume fraction of the solid phase, ϕ^f the volume fraction of the porewater, ρ^s the density of the solid phase, C_j^s the concentration of the solid species j (moles per gram of sediment), M_j^s the molecular mass of the solid species j (moles per gram of species) and S_j^s the reactive surface area per mass of solid species (cm^2 per gram of species).

7.3. Pseudo-solid phase reactions

This class (denoted *sp*) includes "homogeneous" reactions that appear to occur entirely in the solid phase (e.g. recrystallization, pyrite formation). In reality however such reactions effectively proceed via a complex reaction mechanism involving dissolved intermediates. Nonetheless, the overall reaction rate R^{sp} (this time-defined per volume of solid sediment) only incorporates solid concentrations:

$$R^{sp} = k^{sp} \prod_i (C_i^s)^{v_i}. \tag{23}$$

7.4. Precipitation reactions

This class (denoted *pr*) includes heterogeneous reactions driven by the degree of saturation of the porewater fluid with respect to the mineral phase. This dependence upon the saturation state is explicitly included in the rate law R^{pr}(defined per volume of porewater):

$$R^{pr} = k^{pr} \left[\frac{ICP}{K_s^{app}} - 1 \right]^v, \tag{24}$$

where ICP represents the ion concentration product and K_s^{app} denotes the apparent solubility constant of the mineral. The apparent rate constant k^{pr} implicitly incorporates surface area effects, and the catalysing or inhibiting actions of solution constituents.

7.5. Dissolution reactions

Like the precipitation class, the dissolution class of reactions (denoted *ds*) is driven by the saturation state with respect to the corresponding mineral. However, allowing asymmetric precipitation and dissolution, the reaction rate R^{ds}(defined per volume of porewater) is now given by

$$R^{ds} = k^{ds} A_j^s \left[1 - \frac{ICP}{K_s^{app}} \right]^v. \tag{25}$$

As was the case with heterogeneous redox reactions, the rate law, Eq. (25), depends on the reactive surface area A_j^s of the dissolving mineral. Eq. (22) is used to link the reactive surface area to the mineral concentration, which renders the rate law linearly dependent on the concentration of the solid species. This implies that dissolution is stopped when there is no mineral left.

8. The numerical procedure

A MEDIA model consists of n^{spec} partial differential equations (PDEs) of type (3), one for each of the chemical species included by the user in the species set. If m_{ex} denotes the number of reactions added to the extensible reaction set, then each MEDIA model includes $m_{rr} = 18$ reversible (Tables 3 and 4) and $m_{ir} = 12 + m_{ex}$ irreversible reactions (Table 2). As noted previously, the diagenetic system then contains m_{rr} additional unknowns R_k^{rr}. Employing PLEA, this indeterminacy is resolved via the introduction of m_{rr} thermodynamic algebraic equations (AEs, e.g. see Table 10), specifying the local equilibrium conditions for the reversible reactions (Thompson, 1959; Rubin, 1983; Lichtner, 1985). The numerical treatment of the resulting differential algebraic equation (DAE) system involves a two-step procedure. The first step is to rearrange the DAE system by means of a canonical transformation (Aris and Mah, 1963; Smith and Missen, 1982). The actual canonical procedure applied within MEDIA is a modification of the procedure presented by Lichtner (1996) and Steefel and MacQuarrie (1996), and is fully explained in Meysman (2001)[1]. This yields a set of $n^{spec} - m^{rr}$ operational PDEs, which are stated in terms of so-called primary dependent variables (PDVs) and do not longer feature the indeterminate rates R_k^{rr}. Together, the equilibrium AEs and the operational PDEs form a reduced differential algebraic equation (DAE) system, which needs an appropriate integration procedure. Saaltink et al. (2000) advocate the global implicit method—also termed the direct substitution approach (DSA)—for one-dimensional diagenetic problems characterized by highly coupled and non-linear reaction kinetics, and thus, DSA was selected as the preferred integration method within MEDIA. The DSA approach has been widely used in the field of subsurface geochemistry (e.g. Rubin and James, 1973; Valocchi et al., 1981; Jennings et al., 1982; Lewis et al., 1987). The DSA rearranges the DAE system by substitution of the non-linear mass action equations directly into the operational PDEs. As a result, the equilibrium AEs are eliminated and a final set of $n^{spec} - m^{rr}$ non-linear PDEs is obtained.

The numerical solution of the resulting set of non-linear PDEs was implemented by the method-of-lines (MOL) (Byrne and Hindmarsh, 1987; Schiesser, 1991), which replaces the integration domain by a finite number of layers (n^{layer}) and swaps the spatial derivatives for appropriate finite differences. Boudreau (1996a, 1997) discusses the advantages of the MOL for solving early diagenetic problems. MEDIA allows three different types of grids (Fig. 4): (1) an *equally spaced grid* comprising sediment layers of equal thickness (2) an *unequally spaced grid*, to model the sharp gradients that

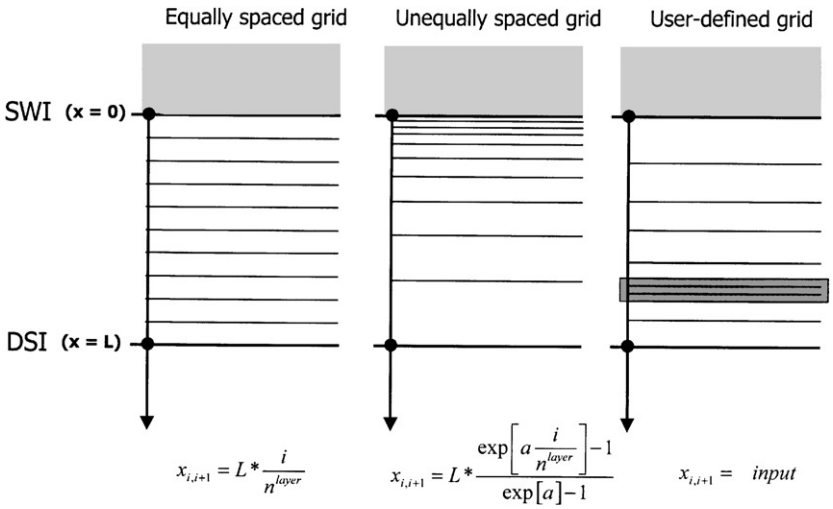

Fig. 4. Overview of different grid types available in MEDIA. Equally spaced grid divides sediment into n^{layer} layers of equal thickness. Unequally spaced grid displays narrowest resolution in uppermost layers of sediment. By setting attenuation constant a, user can control grid resolution of shallow layers relative to deeper layers (in template model accompanying MEDIA package, default value is $a = 3.0$). Distances between layers in user-defined grid are arbitrary and must be provided through an input file.

Table 6
Environmental parameters, grid parameters and parameters determining porosity profile

Environmental parameters		
Temperature	T	279 K
Pressure	P	500 bar
Salinity	S	34.2 PSU
Sediment density	ρ	$2.6\,g\,cm^{-3}$
Sediment flux	F^s	$0.092\,g\,cm^{-2}\,yr^{-1}$
Grid parameters		
Grid type		Unequal
Number of layers	n^{layer}	100 (dimensionless)
Modelled sediment stratum	L	140 cm
Grid attenuation constant	a	3
Porosity profile		
Profile type	—	Exponential (dimensionless)
Porosity at SWI	ϕ_0	0.948 (dimensionless)
Porosity at infinite depth	ϕ_∞	0.824 (dimensionless)
Porosity halving depth	x_ϕ	3.6 cm

Values of environmental parameters were derived from Reimers et al. (1996). Porosity profile was calculated from a profile of resistivity values measured by electrodes also reported in Reimers et al. (1996).

Table 7
Parameters involved in organic matter mineralization

Organic matter fraction	C/N/P ratio	Decay rate constant	Value (yr^{-1})
OM_1	106/16/1.5	k_1^{mi}	2.0
OM_2	106/16/1.5	k_2^{mi}	0.056
OM_3	265/24.5/1	k_3^{mi}	$0.11 \times 10{-}3$
H_2	—	$k_{H_2}^{mi}$	100

The C/N/P ratios of organic matter fractions were constrained by depth profiles of C/N and C/P ratios of total organic matter (i.e. three fractions combined) as reported in Reimers et al. (1996). For the fast and medium degradable fractions, C/N/P ratio approaches Redfield ratio. The higher ratio for the slowly degradable fraction represents the preferential regeneration of N–P substances with depth. First order decay constant of molecular hydrogen is two orders of magnitude higher than decay constant of fast degradable organic matter fraction, reflecting highly reactive nature of molecular hydrogen.

are commonly observed near the SWI and (3) a *user-defined grid*, which is specified via an input file and allows the user to create one or more zones with a higher resolution (e.g. when modelling sapropels and turbidites). In order to obtain both a second-order accurate and stable differencing scheme, a blend of both backward and central differencing is used as proposed by Fiadeiro & Veronis (1977) and applied in Boudreau (1996a) and Soetaert et al. (1996a). Details of the discretization procedure are provided in Meysman (2001). To ensure mass conservation, the discretization method was checked against analytical solutions for simplified model settings (constant porosity, constant biodiffusion coefficient).

In *steady-state calculations*, the time derivatives on the right-hand side of the diagenetic equations (3) are set to zero, and the resulting non-linear system is solved for the concentrations C_i^α. The non-linear solver in MEDIA encapsulates the DNEQF routine from the ISML library, which is based on the MINPACK modification of Powell's hybrid algorithm. This algorithm is a variation of Newton's method, which uses a finite-difference approximation to the Jacobian, and takes precautions to avoid large step sizes or increasing residuals (More et al., 1980). During *dynamic simulations*, the integration is performed by the Backward Differentiation Formula (BDF) method of the stiff ODE-solver package VODE (Brown et al., 1989), using a numerically calculated Jacobian. When performing an *asymptotic run* (i.e. a dynamic simulation until steady state), the stop criterion is based on the error vector $\mathbf{E} = [e_i]$, which is calculated from the array of concentrations $\mathbf{C} = [C_i]$ through $e_i = \delta^R C_i + \delta^A$, where δ^R is a relative tolerance and δ^A an absolute tolerance. The elements of the residuals vector $\mathbf{R} = [r_i]$ are calculated as $r_i = \partial_t C_i / e_i$, where $\partial_t \mathbf{C}$ denotes the rates of change vector of the concentrations. Steady state is reached when the root-mean-square of the residual vector $\mathbf{R}$ drops beneath a preset level. Compared to the direct steady-state calculation, the asymptotic procedure generally requires more runtime. However, a major advantage is that it can start from rough (i.e. guessed) initial conditions.

9. Verification

A two-step verification process was adopted. In a first step, simplified one-species test models were constructed for different types of boundary conditions, which were then compared with analytical solutions, leading to identical results. In a second step, the model description of the STEADYSED code (Van Cappellen and Wang, 1996) was reconstructed within MEDIA and the output was compared for an identical set of boundary conditions and parameter values. The resulting concentration files were identical to the output of the STEADYSED code, except for the pH profiles. The origin of this difference was identified and could be attributed to the different description of sulphide re-oxidation reactions. In STEADYSED, re-oxidation reactions are written in terms of total sulphides, while in MEDIA separate re-oxidation reactions were used for HS^- and H_2S, because MEDIA only allows reactions to be written in terms of

Table 8
Boundary conditions

Species	UBC	Value	Dimensions	LBC	Value	Dimensions
H^+	FC	2.94 E−02	μM	NG	—	—
O_2	FC	1.00 E+01	μM	NG	—	—
H_2	FC	0.00 E+00	μM	NG	—	—
CH_4	FC	0.00 E+00	μM	NG	—	—
NO_3^-	FC	2.50 E+01	μM	NG	—	—
N_2	FC	0.00 E+00	μM	NG	—	—
SO_4^{2-}	FC	2.80 E+04	μM	FC	2.15 E+03	μM
Mn^{2+}	FC	0.00 E+04	μM	NG	—	—
Fe^{2+}	FC	0.00 E+00	μM	NG	—	—
Mg^{2+}	FC	5.32 E+04	μM	NG	—	—
Ca^{2+}	FC	1.03 E+04	μM	FC	4.25 E+03	μM
MnO_2	FF	2.00 E+00	$\mu mol\,cm^{-2}\,yr^{-1}$	NG	—	—
FeOOH	FF	3.60 E+01	$\mu mol\,cm^{-2}\,yr^{-1}$	NG	—	—
OM_1	FF	6.70 E+01	$\mu mol\,cm^{-2}\,yr^{-1}$	NG	—	—
OM_2	FF	6.00 E+01	$\mu mol\,cm^{-2}\,yr^{-1}$	NG	—	—
OM_3	FF	2.48 E+02	$\mu mol\,cm^{-2}\,yr^{-1}$	NG	—	—
$MnCO_3$	FF	0.00 E+00	$\mu mol\,cm^{-2}\,yr^{-1}$	NG	—	—
$CaCO_3$	FF	8.40 E+01	$\mu mol\,cm^{-2}\,yr^{-1}$	NG	—	—
FeS	FF	0.00 E+00	$\mu mol\,cm^{-2}\,yr^{-1}$	NG	—	—
FeS_2	FF	2.00 E+00	$\mu mol\,cm^{-2}\,yr^{-1}$	NG	—	—
C_T	FC	2.45 E+03	μM	FC	2.45 E+04	μM
N_T	FC	5.00 E+01	μM	FC	2.70 E+03	μM
P_T	FC	3.70 E+00	μM	FC	1.60 E+02	μM
S_T	FC	0.00 E+00	μM	FC	7.00 E+03	μM
$\equiv OH_T$	FF	1.00 E+04	$\mu mol\,cm^{-2}\,yr^{-1}$	NG	—	—

Columns 'UBC' and 'LBC' denote type of boundary conditions applied at upper boundary and lower boundary, respectively: FC = fixed concentration, FF = fixed flux, NG = no gradient. All values of concentrations and fluxes were derived from Reimers et al. (1996).

actual chemical species. The latter approach is more consistent, since different amounts of protons will be released upon re-oxidation of HS^- and H_2S.

10. Application

As an illustration of the capabilities of MEDIA, a comprehensive dataset from the Santa Barbara Basin (SBB) was modelled, containing both porewater and solid phase depth profiles as reported in Reimers et al. (1996). For a detailed description of the station locations, the sampling procedures and the analytical techniques, the reader is referred to the latter paper. The aim was to construct a diagenetic model within MEDIA that adequately identifies and integrates the dominant biogeochemical processes in the SBB. Only a brief summary of this modelling exercise is given here. The interested reader is referred to the MEDIA homepage,[2] where this model can be downloaded as a test application. The environmental parameters and the parameters used in grid discretization are summarized in Table 6. The SBB is a modern anoxic basin with

Table 9
Limitation and inhibition constants used in different pathways of organic matter mineralization

	Value	Dimensions
Monod constant		
$K_S^{O_2}$	2 (*)	μM
$K_S^{NO_3^-}$	2 (*)	μM
$K_S^{MnO_2}$	16 (*)	$\mu mol\,g^{-1}$
K_S^{FeOOH}	20 (*)	$\mu mol\,g^{-1}$
$K_S^{SO_4^{2+}}$	1600 (**)	μM
Inhibition constant		
$K_I^{O_2}$	2	μM
$K_I^{NO_3^-}$	2	μM
$K_I^{MnO_2}$	16	$\mu mol\,g^{-1}$
K_I^{FeOOH}	20	$\mu mol\,g^{-1}$
$K_I^{SO_4^{2-}}$	1600	μM

Data on limitation constants were obtained from (*) Van Cappellen and Wang (1996) and (**) Boudreau and Westrich (1984). Inhibition constants were assumed to have same value as limitation constants.

Table 10
Equilibrium constants used in simulation

Equilibrium constant	Value	Units	Equilibrium constant	Value	Units
$K_w = [OH^-][H^+]$	9.93 E−03	$\{\mu M\}^2$	$K_{\equiv NH_4} = \frac{\rho^s \phi^s [\equiv NH_4^+]}{\phi^f [NH_4^+]}$	3.90 E+00	—
$K_C^1 = \frac{[HCO_3^-][H^+]}{[CO_2]}$	9.38 E−01	μM	$K_{\equiv H_2PO_4^-} = \frac{\rho^s \phi^s [\equiv H_2PO_4^-]}{\phi^f [H_2PO_4^-]}$	5.40 E+00	—
$K_C^2 = \frac{[CO_3^{2-}][H^+]}{[HCO_3^-]}$	5.52 E−04	μM	$K_{\equiv H_2PO_4^-} = \frac{\rho^s \phi^s [\equiv H_2PO_4^-]}{\phi^f [H_2PO_4^-]}$	5.40 E+00	—
$K_N = \frac{[NH_3][H^+]}{[NH_4^+]}$	1.17 E−04	μM	$K_{\equiv HPO_4^{2-}} = \frac{\rho^s \phi^s [\equiv HPO_4^{2-}]}{\phi^f [HPO_4^{2-}]}$	5.40 E+00	—
$K_P^2 = \frac{[HPO_4^{2-}][H^+]}{[H_2PO_4^-]}$	7.65 E−01	μM	$K_{\equiv PO_4^{3-}} = \frac{\rho^s \phi^s [\equiv PO_4^{3-}]}{\phi^f [PO_4^{3-}]}$	5.40 E+00	—
$K_P^3 = \frac{[PO_4^{3-}][H^+]}{[HPO_4^{2-}]}$	6.04 E−04	μM	$K_{\equiv Mn^+} = \frac{[\equiv Mn^+]}{[\equiv H][Mn^{2+}]}$	1.00 E−03	μM^{-1}
$K_S = \frac{[HS^-][H^+]}{[H_2S]}$	1.49 E−01	μM	$K_{\equiv Fe^+} = \frac{[\equiv Fe^+]}{[\equiv H][Fe^{2+}]}$	1.00 E−03	μM^{-1}
$K_B = \frac{[B(OH)_4^-][H^+]}{[B(OH)_3]}$	1.50 E−03	μM	$K_{\equiv Mg^+} = \frac{[\equiv Mg^+]}{[\equiv H][Mg^{2+}]}$	1.00 E−03	μM^{-1}
$K_{Si} = \frac{[HSiO_3^-][H^+]}{[H_2SiO_3]}$	1.85 E−04	μM	$K_{CaCO_3} = [Ca^{2+}][CO_3^{2-}]$	1.00 E+00	$\{\mu M\}^2$
$K_{\equiv OH}^1 = \frac{[\equiv OH_2^+][H^+]}{[\equiv OH]}$	1.00 E+00	μM	$K_{MnCO_3} = [Mn^{2+}][CO_3^{2-}]$	1.00 E+00	$\{\mu M\}^2$
$K_{\equiv OH}^1 = \frac{[\equiv OH][H^+]}{[\equiv O^-]}$	1.00 E−03	μM	$K_{FeS} = \frac{[Fe^{2+}][HS^-]}{[H^+]}$	1.00 E+00	μM

Table 11
Kinetic constants used in simulation

	Rate constant	Value ($\mu M^{-1}\,yr^{-1}$)
Fluid redox reactions		
$NH_4^+ + 2O_2 \rightarrow NO_3^- + 2H^+ + H_2O$	k^{fr} [1]	0.500 E−03
$Fe^{2+} + \frac{1}{4}O_2 + \frac{3}{2}H_2O \rightarrow FeOOH + 2H^+$	k^{fr} [2]	0.140 E+00
$H_2S + 2O_2 \rightarrow SO_4^{2-} + 2H^+$	k^{fr} [3]	0.160 E+00
$HS^- + 2O_2 \rightarrow SO_4^{2-} + H^+$	k^{fr} [4]	0.160 E+00
$CH_4 + 2O_2 \rightarrow CO_2 + 2H_2O$	k^{fr} [5]	0.100 E+02
$CH_4 + SO_4^{2-} + 2H^+ \rightarrow CO_2 + H_2S + 2H_2O$	k^{fr} [6]	0.100 E−01
Interface redox reactions		
$4MnO_2 + H_2S + 6H^+ \rightarrow 4Mn^{2+} + SO_4^{2-} + 4H_2O$	k^{ir} [1]	0.172 E−03
$4MnO_2 + HS^- + 7H^+ \rightarrow 4Mn^{2+} + SO_4^{2-} + 4H_2O$	k^{ir} [2]	0.245 E−02
$8FeOOH + H_2S + 14H^+ \rightarrow 8Fe^{2+} + SO_4^{2-} + 12H_2O$	k^{ir} [3]	0.257 E−02
$2FeOOH + HS^- + 5H^+ \rightarrow 2Fe^{2+} + S^0 + 4H_2O$	k^{ir} [4]	0.263 E−01
$\equiv Fe^+ + \frac{1}{4}O_2 + \frac{3}{2}H_2O \rightarrow \equiv H^+ + FeOOH + H^+$	k^{ir} [5]	0.192 E+01
$FeS + H_2S \rightarrow FeS_2 + H_2$	k^{ir} [6]	0.179 E+02
Precipitation reactions		Value ($\mu M\,yr^{-1}$)
$Mn^{2+} + CO_3^{2-} \rightarrow MnCO_3$	k^{pr} [1]	0.100 E−03
$Ca^{2+} + CO_3^{2-} \rightarrow CaCO_3$	k^{pr} [2]	0.267 E−05
$Fe^{2+} + HS^- \rightarrow FeS + H^+$	k^{pr} [3]	0.100 E+00

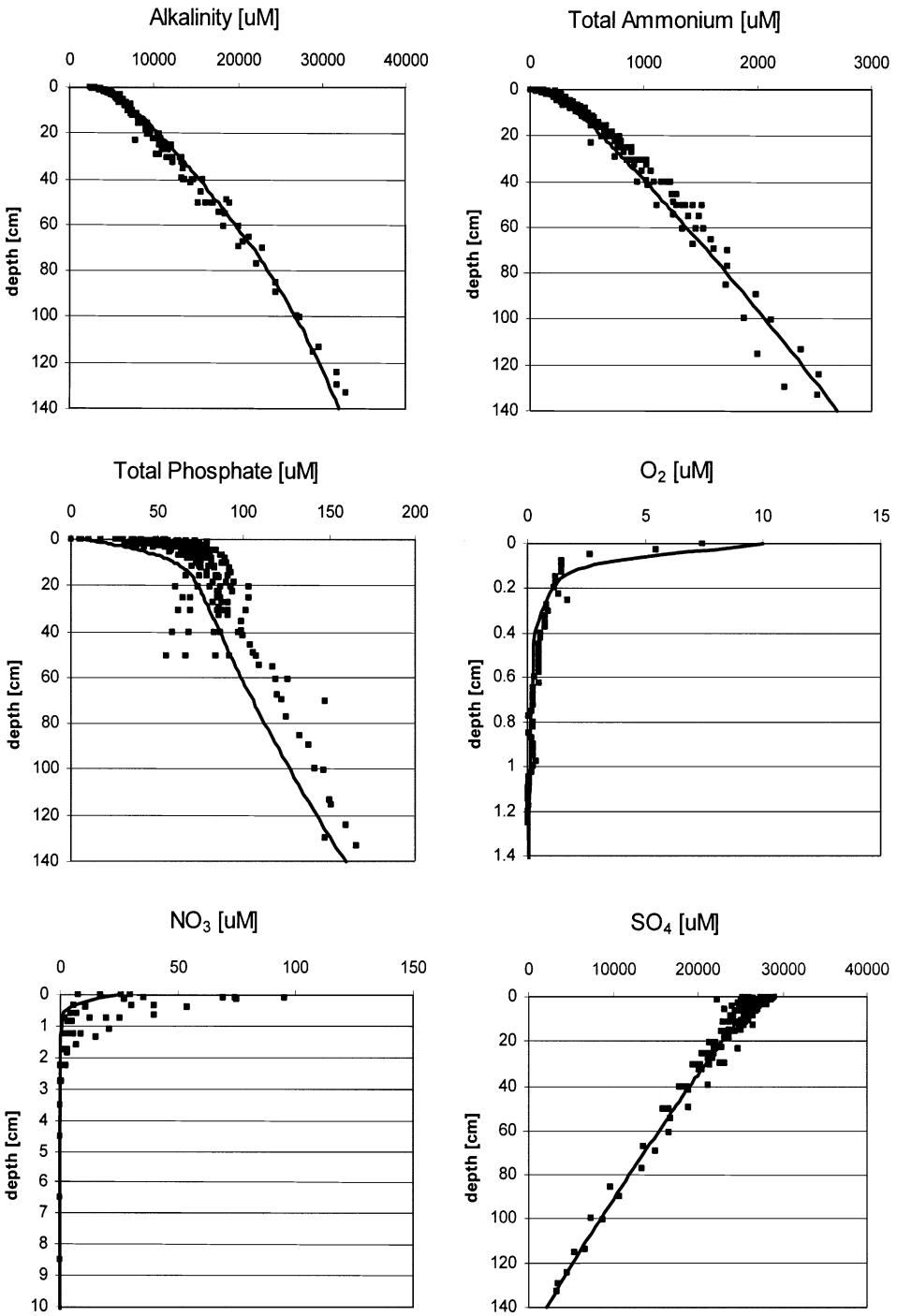

Fig. 5. Diagenetic modelling of solute and solid concentration profiles from Santa Barbara Basin. Continuous lines on graphs are model profiles, points indicate data observations. Solute concentrations expressed in μM (alkalinity, total ammonia, total phosphate, O_2, NO_3, SO_4, Mn^{2+}, Fe^{2+}, Ca^{2+}), solid concentrations (organic matter, FeS and FeS_2) expressed in $\mu mol\, g^{-1}$. Data from Reimers et al. (1996).

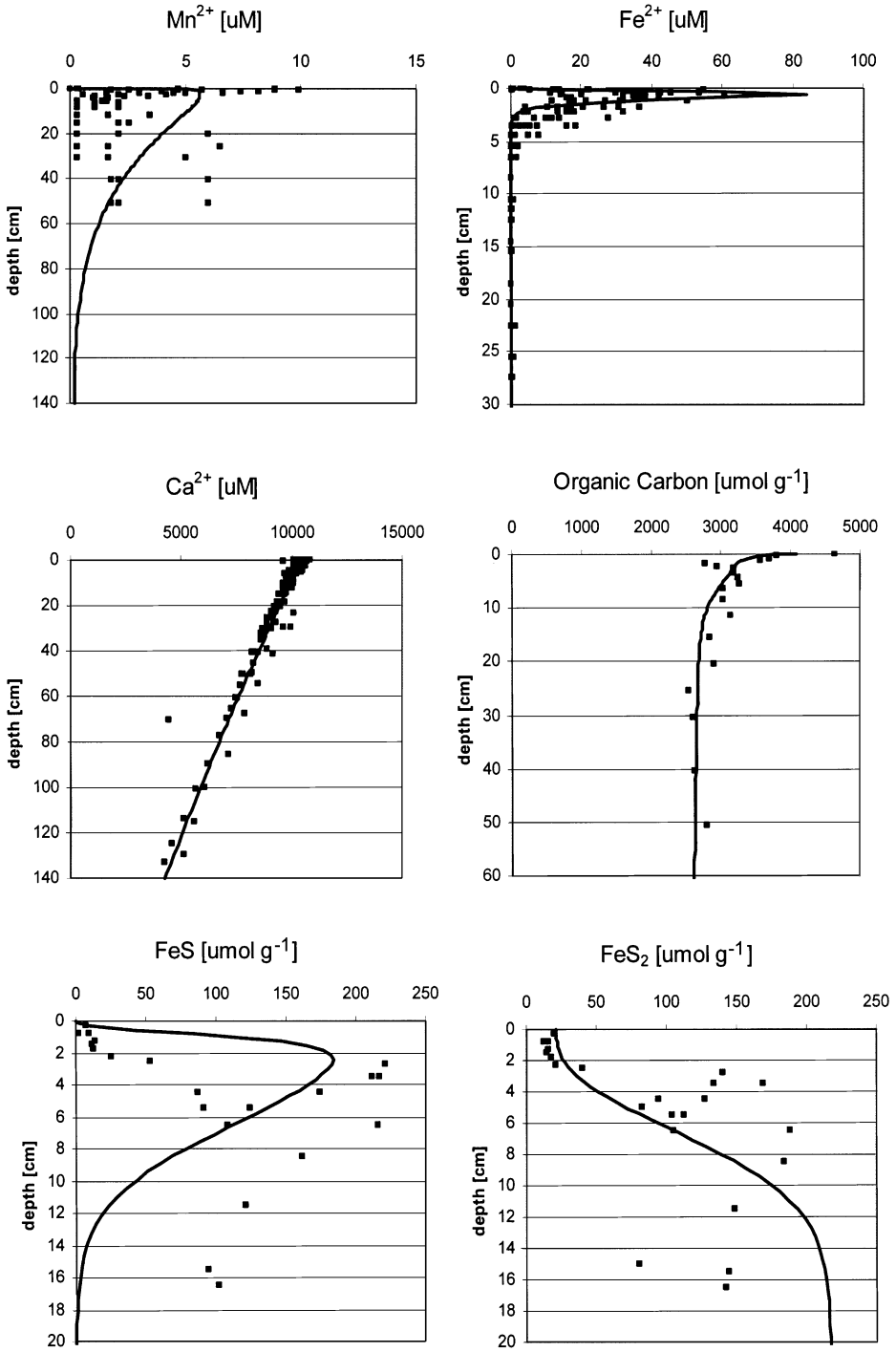

Fig. 5 (*continued*).

varved sediments (Schimmelmann et al., 1990; Reimers et al., 1990), and consequently, no bioturbation or biological irrigation was incorporated in the model. Furthermore, bottom currents in the basin are considered slow, so wave-induced dispersion was equally neglected, while advection and molecular diffusion were considered the dominant transport processes. Organic matter is modelled as three fractions, with different

Table 12
Mineralization pathways in Santa Barbara Basin sediment

Pathway	Rate ($\mu mol\,cm^{-2}\,yr^{-1}$)	Fraction (%)
Oxic respiration	20.7	14.3
Denitrification	28.1	19.4
MnO_2 reduction	1.0	0.7
FeOOH reduction	9.4	6.5
Sulphate reduction	82.3	56.8
Methanogenesis	3.3	2.3
Total	145.0	100

first-order degradation rates and distinct C/N/P ratios, to account for the decreasing reactivity and preferential remineralization of C–N-rich compounds with depth (Table 7). The species set and the associated boundary conditions are shown in Table 8. The reaction set includes the kernel reaction set (Tables 2–4), while fifteen reactions were additionally selected for inclusion in the extensible reaction set. These secondary diagenetic reactions model the reoxidation of reduced byproducts formed in the mineralization of organic matter, the reduction of manganese and iron (hydr)oxides by sulphides, the formation of iron sulphide and pyrite, and the precipitation of manganese and calcium carbonate (Table 11). Extensible reactions were included in a step-wise fashion, starting with the cycling of carbon, nitrogen and phosphorus, and subsequently, extending the model with new reactions involving sulphur, iron and manganese cycling. The values of the equilibrium, Monod/inhibition and other kinetic constants are summarized in Tables 9, 10 and 11, respectively. Fig. 5 compares the steady-state resulting output of the model with the data profiles. The steady-state model profiles of both porewater constituents and solid-phase constituents closely fit the observations, indicating that the model explains a substantial part of the geochemical complexity in the SBB. The model calculates a total mineralization rate (i.e. the combined rate of all three fractions integrated over depth) of $145\,\mu mol\,cm^{-2}\,yr^{-1}$. The rates attributed to the different mineralization pathways are shown in Table 12. Denitrification and sulphate reduction constitute the dominant pathways (19 and 57%, respectively).

11. Conclusion

The aim of the MEDIA project is develop a flexible and extensible software system that provides problem-solving assistance for simulating the biogeochemistry of various types of surface sediments. Here we have reported on the present state of the software, which currently focuses on marine diagenesis. As demonstrated, the present MEDIA software allows user-tailored models to be built from a set of basic building blocks and provides an efficient numerical solution for these models. Future developments will address the modelling of lacustrine systems (i.e. equipping MEDIA with an appropriate activity coefficient model) and a further increase of the flexibility of the reaction set (i.e. to allow the inclusion of an arbitrary number of user-defined reversible reactions).

Acknowledgements

We thank Claire Reimers for her generous supply of the dataset from the Santa Barbara Basin. A substantial part of these ideas have crystallized during fruitful discussions with Bernie Boudreau, while visiting Dalhousie University via the KNAW-grant 'Bezoek aan Buitenlandse Marien-Biologische Instituten'. This study was financially supported by a grant from the Institute for the Promotion of Innovation by Science and Technology in Flanders (IWT) and supported by the European Commission through contract ENV4-CT96-026 (ECOFLAT). This is publication 2985 of the NIOO-KNAW, Centre for Estuarine and Marine Ecology (CEME), Yerseke, the Netherlands.

References

Aller, R.C., 1982. The effects of macrobenthos on chemical properties of marine sediment and overlying water. In: McCall, P.L., Tevesz, M.J.S. (Eds.), Animal-Sediment Relations. Plenum, New York, NY, pp. 53–102.

Aller, R.C., Aller, J.Y., 1998. The effect of biogenic irrigation intensity and solute exchange on diagenetic reaction rates in marine sediments. Journal of Marine Research 56 (4), 905–936.

Aller, R.C., Aller, J.Y., 1992. Meiofauna and solute transport in marine muds. Limnology and Oceanography 37 (5), 1018–1033.

Aller, R.C., Yingst, J.Y., 1985. Effects of the marine deposit-feeders Heteromastus filiformis (Polychaeta), Macoma balthica (Bivalvia), and Tellina texana (Bivalvia) on averaged sediment solute transport, reaction rates, and microbial distribution. Journal of Marine Research 43 (3), 615–645.

Archer, D., Devol, A., 1992. Benthic oxygen fluxes on the Washington Shelf and Slope—a comparison of in situ microelectrode and chamber flux measurements. Limnology and Oceanography 37 (3), 614–629.

Aris, R., Mah, R.H.S., 1963. Independence of chemical reactions. Industrial & Engineering Chemistry Research (I&EC) Fundamentals 2, 90–94.

Bahr, J.M., Rubin, J., 1987. Direct comparison of kinetic and local equilibrium formulations for solute transport affected by surface-reactions. Water Resources Research 23 (3), 438–452.

Bear, J., Bachmat, Y., 1991. Introduction to Modeling of Transport Phenomena in Porous Media. Kluwer Academic Publishers, Dordrecht, The Netherlands, 553pp.

Berner, R.A., 1980. Early Diagenesis. A Theoretical Approach. Princeton University Press, Princeton, NJ, 241pp.

Booch, G., 1994. Object-oriented Analysis and Design with Applications. The Benjamin/Cummings Publishing Company, Inc., San Francisco, CA, 589pp.

Boudreau, B.P., 1984. On the equivalence of nonlocal and radial-diffusion models for porewater irrigation. Journal of Marine Research 42 (3), 731–735.

Boudreau, B.P., Westrich, J.T., 1984. The dependence of sulfate reduction on sulfate concentration in marine sediments. Geochimica et Cosmochimica Acta 48, 2503–2516.

Boudreau, B.P., 1986. Mathematics of tracer mixing in sediments 0.1. spatially dependent, diffusive mixing. American Journal of Science 286 (3), 161–1198.

Boudreau, B.P., 1996a. A method-of-lines code for carbon and nutrient diagenesis in aquatic sediments. Computers & Geosciences 22 (5), 479–496.

Boudreau, B.P., 1996b. The diffusive tortuosity of fine-grained unlithified sediments. Geochimica et Cosmochimica Acta 60 (16), 3139–3142.

Boudreau, B.P., 1997. Diagenetic Models and Their Implementation. Springer, Berlin, 414pp.

Boudreau, B.P., Bennett, R.H., 1999. New rheological and porosity equations for steady-state compaction. American Journal of Science 299 (7–9), 517–528.

Boudreau, B.P., Mucci, A., Sundby, B., Luther, G.W., Silverberg, N., 1998. Comparative diagenesis at three sites on the Canadian continental margin. Journal of Marine Research 56 (6), 1259–1284.

Bowen, R.M., 1976. Theory of mixtures. In: Eringen, A.C. (Ed.), Continuum Physics, Mixtures and EM Field Theories, Vol. III. Academic Press, New York, NY, pp. 1–127.

Brown, P.N., Byrne, G.D., Hindmarsh, A.C., 1989. Vode—a variable-coefficient ODE solver. SIAM Journal on Scientific and Statistical Computing 10 (5), 1038–1051.

Byrne, G.D., Hindmarsh, A.C., 1987. Stiff ODE solvers—a review of current and coming attractions. Journal of Computational Physics 70 (1), 1–62.

Canfield, D.E., Thamdrup, B., Hansen, J.W., 1993. The anaerobic degradation of organic-matter in Danish coastal sediments—iron reduction, manganese reduction, and sulfate reduction. Geochimica et Cosmochimica Acta 57 (16), 3867–3883.

Drobner, E., Huber, H., Wachtershauser, G., Rose, D., Stetter, K.O., 1990. Pyrite formation linked with hydrogen evolution under anaerobic conditions. Nature 346 (6286), 742–744.

Emerson, S., Jahnke, R., Heggie, D., 1984. Sediment–water exchange in shallow-water estuarine sediments. Journal of Marine Research 42 (3), 709–730.

Fiadeiro, M.E., Veronis, G., 1977. Weighted-mean schemes for finite-difference approximation to advection-diffusion equation. Tellus 29 (6), 512–522.

Ford, B., Chatelin, F., 1987. Problem Solving Environments for Scientific Computing. North-Holland, Amsterdam, The Netherlands, 416pp.

Froelich, P.N., Klinkhammer, G.P., Bender, M.L., Luedtke, N.A., Heath, G.R., Cullen, D., Dauphin, P., Hammond, D., Hartman, B., Maynard, V., 1979. Early oxidation of organic-matter in pelagic sediments of the Eastern Equatorial Atlantic—suboxic diagenesis. Geochimica et Cosmochimica Acta 43 (7), 1075–1090.

Gallopoulos, E., Houstis, E.N., Rice, J.R., 1994. Computer as thinker/doer: problem solving environments for computational science. IEEE Computational Science & Engineering 1, 11–21.

Glud, R.N., Fenchel, T., 1999. The importance of ciliates for interstitial solute transport in benthic communities. Marine Ecology-Progress Series 186, 87–93.

Goldberg, E.D., Koide, M., 1962. Geochronological studies of deep-sea sediments by the Io/Th method. Geochimica et Cosmochimica Acta 26, 417–450.

Guinasso, N.L., Schink, D.R., 1975. Quantitative estimates of biological mixing rates in abyssal sediments. Journal of Geophysical Research (Oceans and Atmospheres) 80 (21), 3032–3043.

Harrison, W.D., Musgrave, D., Reeburgh, W.S., 1983. A wave-induced transport process in marine-sediments. Journal of Geophysical Research (Oceans and Atmospheres) 88 (NC12), 7617–7622.

Herman, P.M.J., Soetaert, K., Middelburg, J.J., Heip, C., Lohse, L., Epping, E., Helder, W., Antia, A.N., Peinert, R., 2001. The seafloor as the ultimate sediment trap-using sediment properties to constrain benthic-pelagic exchange processes at the Goban Spur. Deep-Sea Research Part II—Topical Studies in Oceanography 48 (14–15), 3245–3264.

Jeng, D.S., Barry, D.A., Li, L., 2000. Water wave-driven seepage in marine sediments. Advances in Water Resources 24 (1), 1–10.

Jennings, A.A., Kirkner, D.J., Theis, I.L., 1982. Multicomponent equilibrium chemistry in groundwater models. Water Resources Research 18 (4), 1089–1096.

Krom, M.D., Berner, R.A., 1980. Adsorption of phosphate in anoxic marine-sediments. Limnology and Oceanography 25 (5), 797–806.

Lasaga, A.C., 1997. Kinetic Theory in the Earth Sciences. Princeton University Press, Princeton, NJ, 811pp.

Lewis, F.M., Voss, C.I., Rubin, J., 1987. Solute transport with equilibrium aqueous complexation and either sorption or ion-exchange—simulation methodology and applications. Journal of Hydrology 90 (1–2), 81–115.

Lichtner, P.C., 1985. Continuum model for simultaneous chemical reactions and mass transport in hydrothermal systems. Geochimica et Cosmochimica Acta 49, 779–800.

Lichtner, P.C., 1996. Continuum formulation of multicomponent-multiphase reactive transport. In: Lichtner, P.C., Steefel, C.C., Oelkers, E.H. (Eds.), Reactive Transport in Porous Media. The Mineralogical Society of America, Washington, DC, pp. 1–82.

Lovley, D.R., Chapelle, F.H., 1995. Deep subsurface microbial processes. Reviews of Geophysics 33 (3), 365–381.

Mackin, J.E., Aller, R.C., 1984. Ammonium adsorption in marine-sediments. Limnology and Oceanography 29 (2), 250–257.

Madsen, O.S., 1978. Wave-induced pore pressures and effective stresses in a porous bed. Geotechnique 28 (4), 377–393.

Meysman, F.J.R., 2001. Modelling the influence of ecological interactions on reactive transport processes in sediments.

Ph.D. Dissertation, Ghent University, Gent, Belgium, 213pp.

Meysman, F.J.R., Middelburg, J.J., Herman, P.M.J., Heip, C.H.R. 2002. Reactive transport in surface sediments I. model complexity and software quality. Computers & Geosciences, this issue.

Millero, F.J., 1995. Thermodynamics of the carbon-dioxide system in the oceans. Geochimica et Cosmochimica Acta 59 (4), 661–677.

More, J., Garbow, B., Hillstrom, C., 1980. Argonne National Laboratory Report, ANL-80-74.

Mulsow, S., Boudreau, B.P., Smith, J.N., 1998. Bioturbation and porosity gradients. Limnology and Oceanography 43 (1), 1–9.

Ortoleva, P., Merino, E., Moore, C., Chadam, J., 1987. Geochemical self-organization I: reaction-transport feedbacks and modelling approach. American Journal of science 287, 979–1007.

Page-Jones, M., 2000. Fundamentals of Object-Oriented Design in UML. Dorset House Publishing, New York, NY, 458pp.

Rabouille, C., Gaillard, J.F., 1991. Towards the edge—early diagenetic global explanation—a model depicting the early diagenesis of organic-matter, O_2, NO_3, Mn, and PO_4. Geochimica et Cosmochimica Acta 55 (9), 2511–2525.

Reimers, C.E., Lange, C.B., Tabak, M., Bernhard, J.M., 1990. Seasonal spillover and varve formation in the Santa-Barbara Basin, California. Limnology and Oceanography 35 (7), 1577–1585.

Reimers, C.E., Ruttenberg, K.C., Canfield, D.E., Christiansen, M.B., Martin, J.B., 1996. Porewater pH and authigenic phases formed in the uppermost sediments of the Santa Barbara Basin. Geochimica et Cosmochimica Acta 60 (21), 4037–4057.

Rhoads, D.C., 1974. Organism-sediment relations on the muddy sea floor. Oceanography and Marine Biology Annual Review. 12, 263–300.

Rickard, D., Luther, G.W., 1997. Kinetics of pyrite formation by the H_2S oxidation of iron(II) monosulfide in aqueous solutions between 25 and 125 degrees C: the mechanism. Geochimica et Cosmochimica Acta 61 (1), 135–147.

Rosenfeld, J.K., 1979. Ammonium adsorption in nearshore anoxic sediments. Limnology and Oceanography 24 (2), 356–364.

Rubin, J., 1983. Transport of reacting solutes in porous media: relation between mathematical nature of the problem formulation and chemical nature of reactions. Water Resources Research 19 (5), 1231–1252.

Rubin, J., James, R.V., 1973. Dispersion-affected transport of reacting solutes in saturated porous media: Galerkin method applied to equilibrium-controlled exchange in unidirectionally steady water flow. Water Resources Research 9 (5), 1332–1356.

Saaltink, M.W., Carrera, J., Ayora, C., 2000. A comparison of two approaches for reactive transport modelling. Journal of Geochemical Exploration 69, 97–101.

Schiesser, W.E., 1991. The Numerical Method of Lines: Integration of Partial Differential Equations. Academic Press, San Diego, CA, 324pp.

Schimmelmann, A., Lange, C.B., Berger, W.H., 1990. Climatically controlled marker layers in Santa-Barbara Basin sediments and fine-scale core-to-core correlation. Limnology and Oceanography 35 (1), 165–173.

Shum, K.T., Sundby, B., 1996. Organic matter processing in continental shelf sediments—the subtidal pump revisited. Marine Chemistry 53 (1–2), 81–87.

Smith, W.R., Missen, R.W., 1982. Chemical Reaction Equilibrium Analysis. Theory and Algorithms. Wiley, New York, NY, 364pp.

Soetaert, K., Herman, P.M.J., Middelburg, J.J., 1996a. A model of early diagenetic processes from the shelf to abyssal depths. Geochimica et Cosmochimica Acta 60 (6), 1019–1040.

Soetaert, K., Herman, P.M.J., Middelburg, J.J., 1996b. Dynamic response of deep-sea sediments to seasonal variations: a model. Limnology and Oceanography 41 (8), 1651–1668.

Steefel, C.I., MacQuarrie, K.T.B., 1996. Approaches to modeling of reactive transport in porous media. In: Lichtner, P.C., Steefel, C.C., Oelkers, E.H. (Eds.), Reactive Transport in Porous Media. The Mineralogical Society of America, Washington, pp. 83–129.

Thompson, J.B., 1959. Local equilibrium in metasomatic processes. In: Abelson, P.H. (Ed.), Researches in Geochemistry. Wiley, New York, NY, pp. 427–457.

Truesdell, C., Toupin, R., 1960. The classical field theories. In: Flugge, S. (Ed.), Handbuch der Physik. Springer, Berlin, pp. 227–793.

Valocchi, A.J., Street, R.L., Roberts, P.V., 1981. Transport of ion-exchanging solutes in groundwater: chromatographic theory and field simulation. Water Resources Research 17 (5), 1517–1527.

Van Cappellen, P., Gaillard, J.-F., Rabuoille, C., 1993. Biogeochemical transformations in sediments: kinetic models of early diagenesis. In: Wollast, R., Mackenzie, F.T., Chou, L. (Eds.), Interactions of C, N, P and S Biogeochemical Cycles and Global Change. Springer, New York, NY, pp. 401–445.

Van Cappellen, P., Wang, Y.F., 1996. Cycling of iron and manganese in surface sediments: a general theory for the coupled transport and reaction of carbon, oxygen, nitrogen, sulfur, iron, and manganese. American Journal of Science 296 (3), 197–243.

Van der Loeff, M.M.R., 1981. Wave effects on sediment water exchange in a submerged sand bed. Netherlands Journal of Sea Research 15 (1), 100–112.

Wang, Y.F., Van Cappellen, P., 1996. A multicomponent reactive transport model of early diagenesis: application to redox cycling in coastal marine sediments. Geochimica et Cosmochimica Acta 60 (16), 2993–3014.

Westrich, J.T., Berner, R.A., 1984. The role of sedimentary organic-matter in bacterial sulfate reduction—the G model tested. Limnology and Oceanography 29 (2), 236–249.